








Optimization of Building Construction Control System Based on Nonlinear Image Enhancement

Congru Liu¹ , Mingsen Lin² , Kayhan Zrar Ghafoor^{3,4} , Mustafa Zuhaer Nayef Al-Dabagh⁵  and Dimitrios A. Karras⁶ 

¹School of Urban Construction, Wuhan University of Science and Technology, Wuhan, China, liucongru9@gmail.com

²Changjiang Polytechnic, Wuhan, China, linmingsen920@gmail.com

³Department of Computer Science, Knowledge University, Erbil 44001, Iraq, kayhan.zrar@knu.edu.iq

⁴Department of Software & Informatics Engineering, Salahaddin University-Erbil, Erbil 44001, Iraq, kayhan.zrar@knu.edu.iq

⁵Department of Computer Science, Knowledge University, Erbil 44001, Iraq, mustafa.zuhaer@knu.edu.iq

⁶National and Kapodistrian, University of Athens (NKUA), School of Science, Dept. General, Athens, Greece, dakarras@uoa.gr

Corresponding author: Congru Liu, liucongru9@gmail.com

Abstract. To reflect the nonlinear characteristics of the building structural adjustment system, an active vibration control strategy based on the nonlinear is proposed. In this method, the size of the structural control force is determined by comparing the allowable energy with the actual energy, and its direction is determined by taking the derivative of the energy. Because there is no need to solve the linear matrix inequality, the calculation is simple and the operation is convenient. Moreover, when multiple actuators with the same capacity limit are used, the control output force is consistent, thus avoiding the design of multiple control systems and simplifying the controller design. The simulation results show that the maximum controlled displacements of floor 6 to floor 8 are 1.16cm, 1.12cm, and 0.97cm, respectively. The proposed nonlinear energy control method has the advantages of simple control process and avoiding actuator saturation.

Keywords: Nonlinear; Building structure; Structural adjustment of building.

DOI: <https://doi.org/10.14733/cadaps.2023.S3.213-224>

1 INTRODUCTION

Vibration control of nonlinear structures is a hot topic in recent years. The effective control strategies include fuzzy logic control, adaptive control, neural network control and so on. Due to the complex nonlinearity of actual structures, it is difficult to design control laws. In recent years,

it is a research trend to adapt control strategies of linear structures to nonlinear systems, such as improved sliding mode control, improved predictive control, generalized LQG control, etc. [1]. The Bouc-Wen model can be used to describe the nonlinear characteristics of the building structure, and the optimization method is used to design the controller. Although it has a better control effect for high-rise buildings, the order reduction of the model is needed to simplify the controller design. However, the nonlinear model order reduction method is not mature at present, so the optimization design is difficult to achieve. Based on Lyapunov stability theory, a control strategy with good stability was proposed [2-3].

In recent years, a kind of control strategy based on energy has emerged, which can be divided into two kinds: one is the indirect method, such as switching control by changing the substructure or stiffness and damping; one is the direct method. For example, the controller is designed according to the energy distribution. Its disadvantage is that the control force must be determined by the integral, so it is not suitable for real-time control. The development of modern building structures has put forward higher requirements for structural analysis. With the improvement of computing technology, more accurate simulation of real structures has become an increasingly urgent task and requirement. Among the methods of structural seismic analysis, nonlinear time-history analysis is the most accurate and perfect method to simulate the seismic performance of building structures. Due to the limitation of theoretical level and hardware conditions, the early nonlinear time-history analysis used too much simplification, which was contrary to the original intention of accurate simulation. Nowadays, with the development of computing technology and hardware level, it is possible to carry out more accurate nonlinear time history analysis.

At present, the main problems of nonlinear time-history analysis technology are as follows: reinforced concrete simulation, shear wall simulation, selection of nonlinear hysteretic model, calculation, acceleration and result evaluation. Based on the extensive understanding of the research and application frontier of nonlinear time-history analysis technology at home and abroad, this paper introduces the latest development of this technology from the perspective of engineering structure design and focuses on the latest research and application of nonlinear skeleton curve, shear wall simulation, software application and computational convergence acceleration problem. In the past, a lot of work focused on the study of linear model vibration control and simplified the actual structure.

In practice, due to the nonlinear material of the building structure itself, the elastoplasticity of the building structure in the earthquake and the influence of some nonlinear components in the building structure, in addition, the use of hybrid control method introduces some reasons such as the nonlinearity of the base structure in passive control, and finally makes the actual structural control system be nonlinear system. Because of the complexity of nonlinear systems, researchers only started to study them in the last 10 years. Dong P. et al. proposed a strong consensus nonlinear information filter with distributed state estimation for measuring outliers. With state and parameter coupling, the updated equation can be solved by fixed-point iteration. Centralized outliers, powerful information filters are first derived from multiple sensors. It is then extended to a distributed version to merge information from multiple interconnected local estimators [4-5]. Suzuki, T. et al. proposed an effective method for evaluating building safety after an earthquake. The contours and details of the method are described, and experimental results to confirm the accuracy of the method are presented [6]. Saavedra G. et al. believe that expanding the bandwidth of transmission signals is an effective way to increase the overall capacity of optical fibers. The effect of expanding the transmission bandwidth on optical communication system is experimentally studied with the reachable rate as the performance index. The tradeoff between large bandwidth and high nonlinear interference (NLI) noise is analyzed experimentally and theoretically. The growth of NLI noise in the 40 GHz to 7.3 THz band is studied by 64 QAM and Nyquist pulse shaping technique. With the increase of signal bandwidth, the logarithmic growth of NLI noise is consistent with the prediction of Gaussian noise model [7-8].

To sum up, this paper proposes a simple and effective new control method, the idea is as follows: (1) Calculate the allowable energy of the structure according to the allowable

displacement and velocity of the building floor; (2) Calculate the actual energy of the structure according to the estimated displacement and velocity of the measurement; (3) Compare the allowable energy with the actual energy to determine the size of the control force; (4) The direction of control force is determined according to Lyapunov function. The proposed method has the following advantages: (1) For multiple actuators with the same capacity limit, the control force output is consistent, which can greatly simplify the controller design; (2) Because the energy is allowed to be set in advance, only the actual energy is needed to calculate, the control force is easy to determine, the step control is adopted, and the control process is simple; (3) The structure does not need order reduction. Finally, a computational example is given to illustrate the effectiveness of the method.

2 RESEARCH METHODS

2.1 Nonlinear Control Theory

Feedback linearization methods can be further divided into feedback linearization methods based on differential geometry (input -to-state feedback linearization, input and output linearization), direct feedback linearization, and inverse system methods. At present, it has not been used in structural vibration control. Compared with the approximate linearization method, this method has a good prospect and is an accurate linearization method. The drawback is the need for accurate modeling. Variable structure control (VSC) can be divided into two types: one is to transform the structure into a linear system and then use the linear VSC; the other is to design the VSC law directly on the basis of the nonlinear model. At present, it is generally the former, which does not make full use of the robustness of nonlinear variable structure control. Such as variable stiffness and variable damping control.

The Lyapunov direct control method can also be divided into two kinds. One is to use the linear Lyapunov direct control method by first transforming the structure into a linear system, and the other is to directly design the Lyapunov direct control method for the nonlinear model. At present, it is also the former kind.

2.2 Structural Analysis Model

2.2.1 Nonlinear model

Figure 1 shows the nonlinear interlinear shear model system. By adopting the Wen-Bouc restoring force model, the restoring force $F_{si}(x_i)$ of layer i is:

$$F_{si}(x_i) = \bar{\alpha}_i k_i x_i + (1 - \bar{\alpha}_i) k_i D_{yi} V_i \quad (2.1)$$

Where $\bar{\alpha}$ is the ratio of the post-yield stiffness to the preyield stiffness of the I layer; k_i is the elastic stiffness of the I layer; D_{yi} is the ultimate yield displacement of the i th layer, which is constant; v_i is a dimensionless variable, represents the hysteretic component of the deformation of the 'layer' of the structure, and is:

$$\dot{v} = D_{yi}^{-1} \left[A_i \dot{x}_i - \beta_i |\dot{x}_i| |v_i|^{n_i-1} v_i - y_i \dot{x}_i |v_i|^{n_i} \right] = f_i(\dot{x}_i, v_i) \quad (2.2)$$

A_i 、 β_i 、 y_i 、 n_i are constants related to the shape of the hysteretic loop.

The structural equation can be expressed as:

$$M\ddot{X}(t) + C\dot{X}(t) + K_e X(t) + K_f V(t) = M I_0 \ddot{X}_0 + H U \quad (2.3)$$

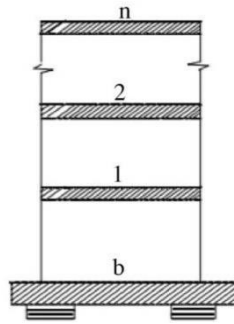


Figure 1: N layer nonlinear structure.

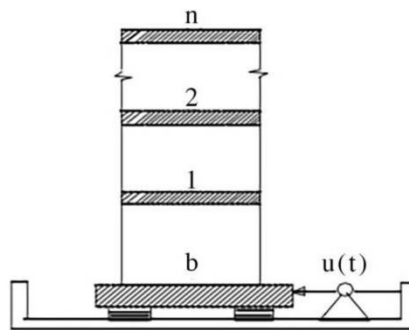


Figure 2: Calculation example diagram.

Where $X = (x_1, x_2, \dots, x_n)$ is the displacement vector between layers of the structure; $\dot{X} = (\dot{x}_1, \dot{x}_2, \dots, \dot{x}_n)$ is the velocity vector between layers of the structure; $\ddot{X} = (\ddot{x}_1, \ddot{x}_2, \dots, \ddot{x}_n)$ is the interlayer acceleration vector of each layer of structure. $V = (v_1, v_2, \dots, v_n)$ is the relative hysteresis vector between each layer; M is the $n \times n$ dimension mass matrix corresponding to X ; \ddot{X}_0 is the acceleration of ground motion; seismic acceleration position vector $I_0 = [1, 1, \dots, 1]^T$; H is the position matrix of $n \times r$ -dimensional controller; K_e is the $n \times n$ dimension stiffness matrix relative to X ; K_f is the hysteretic stiffness matrix relative to V ; C is the damping matrix for the velocity vector \dot{X} ; U is the $(r \times 1)$ -dimensional control force vector.

For the structure shown in Figure 1, $M(i, j) = m_i, i \geq j$; The rest of the elements are zero. $C(i, i) = c_i, i = 1 \sim n$; $C(i, i+1) = -c_{i+1}$. The rest of the elements are zero. $K_e(i, i) = \bar{\alpha}_i k_i, i = 1 \sim n$; $K_e(i, i+1) = -\bar{\alpha}_{i+1} k_{i+1}, i = 1 \sim n-1$. The rest of the elements are zero. $K_f(i, i) = (1 - \bar{\alpha}_i) k_i D_{yi}, i = 1 \sim n$; $K_f(i, i+1) = -(1 - \bar{\alpha}_{i+1}) k_{i+1} D_{y_{i+1}}, i = 1 \sim n-1$; The remaining elements are zero [9].

Make $\hat{Z} = [XV\dot{X}]^T$, Transform the original equation (2.2) into the equation of state:

$$\hat{Z} = \hat{g}[\hat{Z}(t)] + \hat{B}U(t) + \hat{W}_1\ddot{X}_0(t) \quad (2.4)$$

2.2.2 Elastoplastic second-order stiffness matrix of frame structures

Steel frame of the basic component is Yuan, adopting Giberson single component model, to describe the nonlinear working condition of the rod, Yuan assuming that the nonlinear concentration at the end of the bar, with a two nonlinear spring rods to consider the bar into a state of material nonlinearity, considering the bending deformation, shear deformation, axial force of the second order effect, can deduce the frame beams and columns of the second order elastic-plastic element stiffness matrix Array as follows:

$$[K]^{(e)} = [K]_e^{(e)} - \frac{N}{l} [K]_g^{(e)} [K]_p^{(e)} \quad (2.5)$$

Where: $[K]_e^{(e)}$ elastic element stiffness matrix, $[K]_g^{(e)}$ geometric element stiffness matrix, $[K]_p^{(e)}$ plastic stiffness matrix.

2.2.3 Elastoplastic second-order stiffness matrix of the supporting structure element

Braced structure types are commonly used in steel structures. Most of the research work at home and abroad focuses on the bearing capacity of the braced structures, the influence of braced structures on the lateral stiffness of structure, and the restoring force characteristics of the braced structures. The analysis model of braced structure used for dynamic analysis is rarely introduced in domestic and foreign literatures. The reinforced concrete shear wall structure has the closest mechanical performance to the supporting structure. In the 1980s, when Japan and the United States jointly studied the nonlinear seismic response of reinforced concrete frame-shear walls, the three-vertical line element model was adopted: The bending deformation and shearing deformation of the wall are respectively represented by the bending spring and the shearing spring located on the central axis of the wall. The upper and lower parts of the wall on the same layer are simplified as rigid rods. The side columns of the wall are represented by two articulated connecting rods. The model can well simulate the nonlinear state of the bending deformation, shear deformation and axial deformation of the side pillar under the earthquake action. Using it for reference, a three-element model is introduced for the steel braced structure, that is, the bending deformation, shear deformation and axial deformation of the steel braced structure are respectively represented by the bending spring, shear spring and axial spring located at the central axis of the braced structure. In this model, the flexural stiffness is provided by the columns on both sides of the supporting structure, the shear stiffness is provided by the bracing, and the axial stiffness is naturally provided by the columns on both sides. To be able to apply the single component model for analysis, the bend is divided by the spring on the upper and lower sides, and the distance from the bar end is zero. According to the principle of strain energy and the variational method, after obtaining the first-order element stiffness matrix of this model, the Giberson single-component model is also adopted. After the same derivation process as the frame, the second-order elastoplastic element stiffness matrix of the supporting structure can be obtained as follows:

$$[K]_b^{(e)} = [K_b]_e^{(e)} - \frac{N}{h} [K_b]_g^{(e)} - [K_b]_p^{(e)} \quad (2.6)$$

Where, $[K_b]_e^{(e)}$ 、 $[K_b]_g^{(e)}$ 、 $[K_b]_p^{(e)}$ are respectively elastic element stiffness, matrix geometric element stiffness, matrix and plastic element stiffness matrix of the supporting structure [10-11].

2.2.4 Resilient force characteristics of structures

The structure will enter the elastic-plastic stage under earthquake, so it is necessary to understand the restorative force characteristics of the structure. Since the restorative force characteristics of frame structures are widely understood, the braced frame is mainly introduced

here. The hysteresis curve of the frame under the reciprocating horizontal load is stable spindle-shaped, and the hysteresis curve of the support under the reciprocating horizontal load is an inverse S-shaped deterioration due to the repeated compression and buckling of the rods. A braced frame is a composite structure composed of a frame and braces. Its hysteretic curve is not a simple superposition of the two hysteretic curves, but has the characteristics of a composite structure. When the deformation of reciprocating loading is controlled at a small value, the support bars participate in the compression effectively, and the support has higher resistance and stiffness. When the deformation range is large, the stiffness and resistance of the bracing will gradually decrease with the increase of the number of cycles due to the repeated buckling of the bracing bars.

2.3 Structural Nonlinear Model

Set the N-story building structure model with an actuator as Figure 3, and the vibration equation under earthquake action can be expressed as:

$$M\ddot{X}(t) + F_c[\dot{X}(t)] + F_k[X(t)] = -M\ddot{x}_g + Bu(t) \quad (2.7)$$

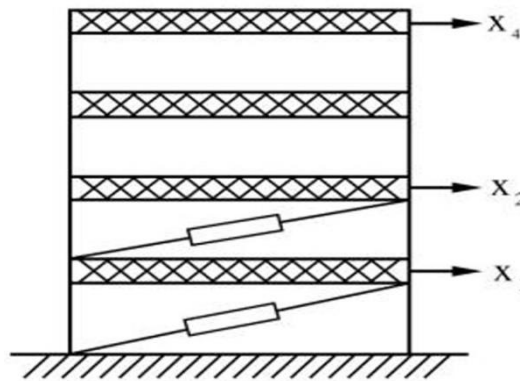


Figure 3: A building model with an actuator.

Type: $X = [x_1, x_2, \dots, x_n]^T$ is the displacement of each floor relative to the ground; M is the diagonal mass matrix; $F_c[\dot{X}(t)]$ is the structural damping force vector. In this paper, it is assumed to be viscous damping, that is: $F_c[\dot{X}(t)] = C\dot{X}(t)$, C is the damping matrix; $F_k[X(t)]$ is the structural restoring force vector; I is a column vector composed of 1; \ddot{x}_g is the acceleration of seismic wave; B is the position matrix of the actuator; B is the position matrix of the actuator; I is the matrix of order $N \times P$, u is the control force vector of dimension $P \times 1$, and is the number of actuators [12-13].

Here, the Bouc-Wen model is adopted to describe the restorative force, and the restorative force of the i th layer can be expressed as:

$$F_{ki}[X(t)] = \alpha_i k_i y_i + (1 - \alpha_i) k_i d_i w_i \quad (2.8)$$

Where, $y_i = x_i - x_{i-1}$ is interlayer displacement; α_i is the ratio of the post-yield stiffness to the periled stiffness of the I layer; k_i is the elastic stiffness; d_i is the ultimate yield displacement; w_i is a dimensionless variable, which can be expressed as:

$$\dot{w}_i = g(\dot{y}_i, w_i) = \left(\theta_i \dot{y}_i - \beta_i |\dot{y}_i| |w_i|^{n_i-1} w_i - \gamma_i \dot{y}_i |w_i|^{n_i} \right) / d_i \quad (2.9)$$

Type: $\theta_i, \beta_i, \gamma_i, n_i$; are the parameters related to the hysteretic loop curve. For a single-story building, when $m=450000\text{kg}$, $k=18.5 \times 10^6 \text{N/m}$, $c=26170 \text{N}\cdot\text{s/m}$, $d=0.04$, $\alpha=0.01$, $\theta=1$, $\beta=0.5$, $n=3$, $\gamma=0.5$, the hysteretic loop curve is shown in Figure 4.

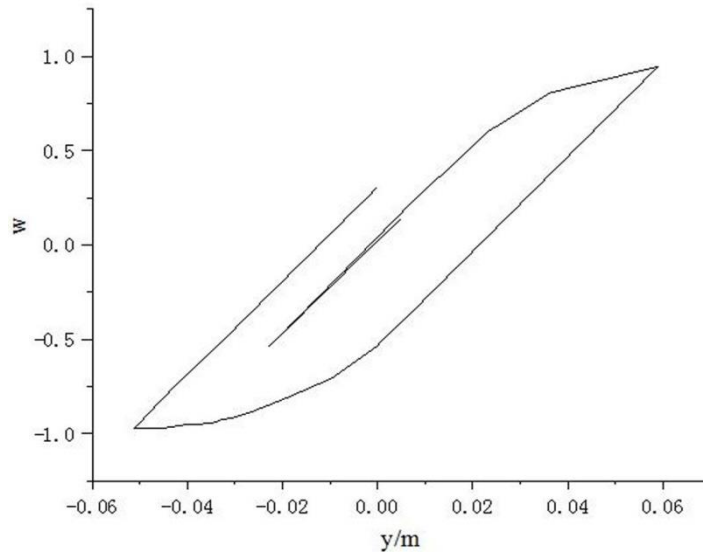


Figure 4: Short, centered caption, terminated with a full stop.

Eq. (2.7) is now converted into a vibration equation expressed in terms of interlayer displacement

$$\bar{M}\ddot{Y} + C\dot{Y} + K_1 Y + K_2 W = -M\ddot{x}_g + Bu(t) \quad (2.10)$$

Type: $Y = [y_1, y_2, \dots, y_n]^T$; $\bar{M}(i, j) = m_i, i \geq j$. The rest of the elements are zero; $C(i, i) = c_i, i = 1, \dots, n, n-1$; The rest of the elements are zero; $K_1(i, i) = \alpha_i k_i, i = 1, \dots, n, K_1(i, i+1) = -\alpha_{i+1} k_{i+1}, i = 1, \dots, n-1$; The rest of the elements are zero; $K_2(i, i) = (1 - \alpha_i) k_i d_i, i = 1, \dots, n, K_2(i, i+1) = -(1 - \alpha_{i+1}) k_{i+1} d_{i+1}, \dots, n-1$. The rest of the elements are zero; $W = [w_1, w_2, \dots, w_n]^T$

Transform Equation (2.10) into an equation of state, as follows:

$$\dot{Z}(t) = F[Z(t)] + Gu(t) + E\ddot{x}_g \quad (2.11)$$

Type

$$Z = \begin{bmatrix} Y \\ W \\ \dot{Y} \end{bmatrix}, F = \begin{bmatrix} \dot{Y} \\ g(\dot{Y}, W) \\ -\bar{M}^{-1}(C\dot{Y} + K_1 Y + K_2 W) \end{bmatrix},$$

$$G = \begin{bmatrix} 0 \\ 0 \\ \bar{M}^{-1}B \end{bmatrix}, E = \begin{bmatrix} 0 \\ 0 \\ -\bar{M}^{-1}MI \end{bmatrix}$$

2.4 Control Algorithm

The energy distribution of the structure under earthquake action obeys Rayleigh probability distribution, and its density function can be expressed as

$$p(E) = \frac{\pi(E - E_{\min})}{2(\bar{E} - E_{\max})^2} \exp\left(\frac{\pi(E - E_{\min})^2}{4(\bar{E} - E_{\min})^2}\right) \quad (2.12)$$

$$E = \frac{1}{2} \bar{Z}^T Q \bar{Z} \quad (2.13)$$

$$Q = \text{diag}(K, M) \quad (2.14)$$

Where, E_{\min} is the minimum energy of the structure; \bar{E} is the average energy; $\bar{Z} = [Y^T, \dot{Y}^T]^T$; K and M are respectively the mass and stiffness matrices of the structure [17-18].

The control force can be determined by integrating Equation (2.12). For the nonlinear vibration studied in this paper, the integration is difficult to achieve, namely, the numerical solution method is adopted, and the calculation time is long, which is not good for real-time control. In addition, the stiffness matrix K in Equation (2.14) has no explicit expression in the vibration equation (2.10). For this reason, a linear control strategy is developed. The energy is still calculated according to Equation (2.13), but Equation (2.14) is changed

$$Q = \text{diag}(\bar{K}, \bar{M}) \quad (2.15)$$

Where \bar{K} is the same as K , just take $\alpha_i = 1, i = 1, \dots, n$.

In Equation (2.13), \bar{Z} is the state variable, which is related to the interstate displacement and the horizontal velocity of the building. It is assumed that the allowable values of the interstate displacement and the horizontal velocity of the building are respectively

$$\Delta_0 = [\delta_1, \delta_2 \dots, \delta_n]^T \quad (2.16)$$

$$\dot{\Delta}_0 = [\dot{\delta}_1, \dot{\delta}_2 \dots, \dot{\delta}_n]^T \quad (2.17)$$

The allowable vibration energy of the structure is defined as follows:

$$E_c = \frac{1}{2} \bar{Z}_c^T Q \bar{Z}_c \quad (2.18)$$

$$\bar{Z}_c = \begin{bmatrix} \Delta_0 \\ \dot{\Delta}_0 \end{bmatrix} \quad (2.19)$$

At time t , the actual vibration energy of the structure can be obtained by substituting the measured signal into Equation (2.7). Let it be E_t , and then the control force defined in this paper is as follows:

$$\rho = \begin{cases} E_t / E_c, E_c \geq E_t \\ 1, E_c < E_t \end{cases} \quad (2.20)$$

The output force adopts the step function, that is, when calculating the next control force, the current control force remains unchanged, and the control force of the JTH actuator is:

$$u_j = \rho \circ u_j^{\max}, j = 1, 2, \dots, p \quad (2.21)$$

where, u_j^{\max} is the maximum control force allowed by the JTH actuator. According to the definitions of Equations (2.20) and (2.21), when the actual vibration energy of the structure is less than or equal to the allowable energy, the control force is less than or equal to the capacity limit of the actuator. When it is larger than the allowable energy, the maximum control force of the actuator is used for vibration control. If the allowable energy value is smaller, the probability of the maximum control force in the control process is greater, and the control effect is certainly relatively good. The allowable energy calculated by Equation (2.18) is the only suggested value used in the design. Considering that only the allowable value of interstate displacement but no allowable value of floor horizontal velocity may be encountered in the actual design, the following equation can also be used to calculate the allowable energy:

$$E_c = \frac{1}{2} \Delta_0^T K \Delta_0 \quad (2.22)$$

At this point, the mass matrix must be zero when using Equation (2.13) to calculate the actual energy. If you want a better control effect, you can lower the allowable energy based on the design. Equation (2.21) only defines the magnitude of the control force, and its direction can be determined according to the design concept of Lyapunov controller. The direction of the control force can be defined as:

$$\text{sgn}(u^T) = -\text{sgn}(\dot{Y}^T B) \quad (2.23)$$

Where $\text{sgn}(\circ)$ is a symbolic function [14].

3 RESULT ANALYSIS

The model is an eight-story shear-type building, and its model parameters are: $m_i = 345600\text{kg}$; $\theta_i = 1$; $\beta_i = 0.5$; $\gamma_i = 0.5$; $n_i = 95$; $\alpha_i = 0.1$; $i = 1, 2, \dots, 8$; The remaining parameters are shown in Table 1.

i	$k_i / N^\circ m^{-1}$	d_i / m	$c_i / N^\circ s^\circ m^{-1}$
1	3.40×10^8	0.024	4.90×10^5
2	3.26×10^8	0.023	4067×10^5
3	2.85×10^8	0.022	4.10×10^5
4	2.69×10^8	0.021	3.86×10^5
5	2.43×10^8	0.020	3.48×10^5
6	2.07×10^8	0.019	2.98×10^5
7	1.69×10^8	0.017	2.43×10^5
8	1.37×10^8	0.015	1.96×10^5

Table 1: Building parameters.

The maximum output force of the five floors above is 3000kN, and that of the three floors below is 2000kN [15-16]. Assuming that only the allowable values of the interlayer displacement of each building are known, the allowable energy calculated according to Equation (16) is 6120J, the seismic wave is Elcentro (NS) wave, and the control time is 6s. MATLAB software was used for simulation, and the equation of state (11) was calculated using ODE23 (i.e., the second-order Runge-Kutta method). Since the lower three floors have the same control force and the upper five floors have the same control force, it is only necessary to draw two control force schedule diagrams [17].

The displacement between floors is adopted, and there is little difference in the control effect of each floor. For example, the control effect of floor 7 is shown in Figure 5 (in the figure, the dashed line is the displacement after control, and the solid line is the displacement without control).

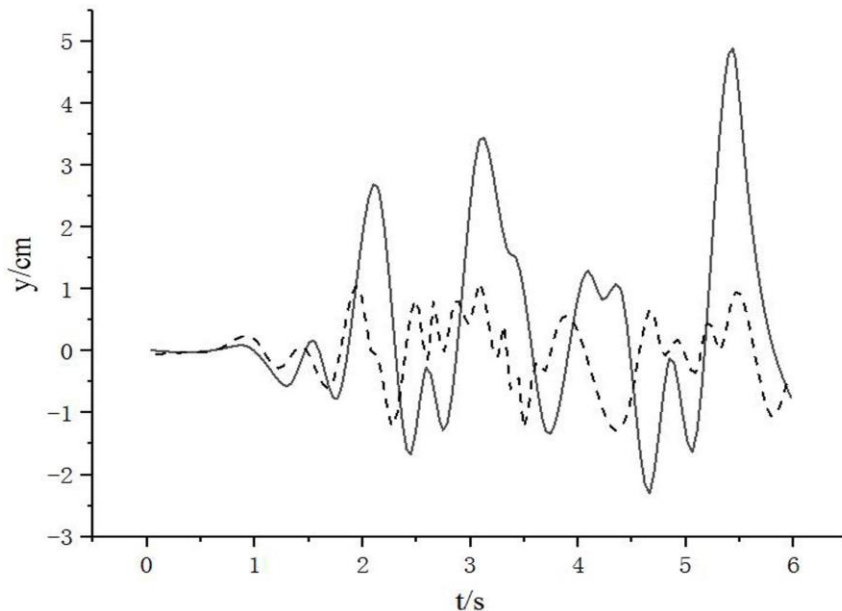


Figure 5: Control effect of floor 5.

It can be seen from the figure that the vibration is well controlled, and the better control effect can be obtained by increasing the control force. The control results for floors 6 to 8 are shown in Table 2.

Floor	There is no control/ cm	Active control/ cm
6	3.64	1.32
7	4.79	1.27
8	1.97	1.00

Table 2: Maximum layer displacement under earthquake action.

If the allowable value of the interlayer displacement of each building is reduced, assuming that half of the above value is taken, the maximum controlled displacements of floors 6 to 8 are 1.16cm, 1.12cm and 0.97cm respectively. Although the control effect is better, the frequency of the maximum control force is higher and it is easy to cause the damage of the control.

4 CONCLUSIONS

Vibration control of large structures often requires large control forces. Due to economic reasons, the output force provided by the actuator is often less than the design control force, which leads to a saturation phenomenon in the control process. The proposed nonlinear energy control method has the advantages of simple control process and avoiding actuator saturation. However, there are also disadvantages: in the simulation, it is found that it is difficult to achieve the control purpose if 1-2 actuators are used; in addition, when there are more than 4 actuators, it can be easily adjusted and the desired control effect can be obtained. The specific reasons need further research.

Congru Liu, <https://orcid.org/0000-0002-2062-1280>

Mingsen Lin, <https://orcid.org/0000-0002-8693-2583>

Kayhan Zrar Ghafoor, <https://orcid.org/0000-0001-9046-9475>

Mustafa Zuhaer Nayef Al-Dabagh, <https://orcid.org/0000-0001-8938-5258>

Dimitrios A. Karras, <https://orcid.org/0000-0002-2759-8482>

REFERENCES

- [1] Li Tan; Jiang, J.: Adaptive Volterra filters for active control of nonlinear noise processes, IEEE Transactions on Signal Processing, 49(8), 2021, 1667–1676. <https://doi.org/10.1109/78.934136>
- [2] Cui, J.; Hong, J.; Liu, Z.; Zhou, W.: Strong convergence rate of splitting schemes for stochastic nonlinear Schrödinger equations, Journal of Differential Equations, 266(9), 2019, 5625–5663. <https://doi.org/10.1016/j.jde.2018.10.034>
- [3] Wang, H.; Sharma, A.; Shabaz, M.: Research on digital media animation control technology based on recurrent neural network using speech technology, International Journal of System Assurance Engineering and Management, 13(1), 2022, 564–575. <https://doi.org/10.1007/s13198-021-01540-x>
- [4] Sun, Y.; Li, H.; Shabaz, M.; Sharma, A.: Research on building truss design based on particle swarm intelligence optimization algorithm, International Journal of System Assurance Engineering and Management, 13(1), 2022, 38–48. <https://doi.org/10.1007/s13198-021-01192-x>
- [5] Saavedra, G.; Tan, M.; Elson, D. J.; Galdino, L.; Semrau, D.; Iqbal, M. A.; Bayvel, P.: Experimental analysis of nonlinear impairments in fibre optic transmission systems up to 7.3 THz, Journal of Lightwave Technology, 35(21), 2017, 4809–4816. <https://doi.org/10.1109/JLT.2017.2760138>
- [6] Kothai, G.; Poovammal, E.; Dhiman, G.; Ramana, K.; Sharma, A.; AlZain, M. A.; Gaba, G.S.; Masud, M.: A New Hybrid Deep Learning Algorithm for Prediction of Wide Traffic Congestion in Smart Cities. Wireless Communications and Mobile Computing, 2021, 2021, 1–11. <https://doi.org/10.1155/2021/5583874>
- [7] Dong, P.; Jing, Z.; Leung, H.; Shen, K.; Li, M.: Robust Consensus Nonlinear Information Filter for Distributed Sensor Networks With Measurement Outliers, IEEE Transactions on Cybernetics, 49(10), 2019, 3731–3743. <https://doi.org/10.1109/TCYB.2018.2850368>
- [8] Dogra, J.; Jain, S.; Sharma, A.; Kumar, R.; Sood, M.: Brain tumor detection from MR images employing fuzzy graph cut technique, Recent Advances in Computer Science and Communications (Formerly: Recent Patents on Computer Science), 13(3), 2020, 362–369. <https://doi.org/10.2174/2213275912666181207152633>
- [9] Suzuki, T.: Mode selection method in modal iterative error correction for stabilization of convergence, Journal of Structural and Construction Engineering (Transactions of AIJ), 84(756), 2019, 195–203. <https://doi.org/10.3130/aijs.84.195>
- [10] Li, G.; Liu, F.; Sharma, A.; Khalaf, O.I.; Alotaibi, Y.; Alsufyani, A.; Alghamdi, S.: Research on the Natural Language Recognition Method Based on Cluster Analysis Using Neural Network, Mathematical Problems in Engineering, 2021, 2021, 1–9. <https://doi.org/10.1155/2021/9982305>

- [11] Saavedra, G.; Tan, M.; Elson, D. J.; Galdino, L.; Semrau, D.; Iqbal, M. A.: Experimental analysis of nonlinear impairments in fibre optic transmission systems up to 7.3 thz, *Journal of Lightwave Technology*, 35(21), 2019, 4809-4816. <https://doi.org/10.1109/JLT.2017.2760138>
- [12] Balyan, V.: Channel Allocation with MIMO in Cognitive Radio Network, *Wireless Personal Communication*, 116, 2021, 45-60. <https://doi.org/10.1007/s11277-020-07704-5>
- [13] Levin, L. Yu.; Semin, M. A.; Zaitsev, A. V.: Adjustment of Thermophysical Rock Mass Properties in Modeling Frozen Wall Formation in Mine Shafts under Construction, *Journal of Mining Science*, 55(1), 2019, 157-168. <https://doi.org/10.1134/S1062739119015419>
- [14] Shao, Y.; Wu, J.; Ou, H.; Pei, M.; Liu, L.; Movassagh, A.A.; Sharma, A.; Dhiman, G.; Gheisari, M.; Asheralieva, A.: Optimization of Ultrasound Information Imaging Algorithm in Cardiovascular Disease Based on Image Enhancement, *Mathematical Problems in Engineering*, 2021, 2021, 1-8. <https://doi.org/10.1155/2021/5580630>
- [15] Rathee, G.; Sharma, A.; Saini, H.; Kumar, R.; Iqbal, R.: A hybrid framework for multimedia data processing in IoT-healthcare using blockchain technology, *Multimedia Tools and Applications*, 79(15), 2020, 9711-9733. <https://doi.org/10.1007/s11042-019-07835-3>
- [16] Singh, A.; Ahuja, H.; Bhadoria, V.; Singh, S.: Control Implementation of Squirrel Cage Induction Generator based Wind Energy Conversion System, 2020. <https://doi.org/10.1063/5.0043408>
- [17] Kobro-Flatmoen, A.; Witter, M. P.: Neuronal chemo-architecture of the entorhinal cortex: A comparative review, *European Journal of Neuroscience*, 50(10), 2019, 3627-3662. <https://doi.org/10.1111/ejn.14511>